


# Symmetry breaking in minimum dissipation networks

Aarathi Parameswaran <sup>1,2</sup> Iva Bačić <sup>1,3</sup> Andrea Benigni <sup>1,4</sup> and Dirk Witthaut <sup>1,5,\*</sup>

<sup>1</sup>*Institute of Climate and Energy Systems: Energy Systems Engineering (ICE-1),  
Forschungszentrum Jülich, 52428 Jülich, Germany*

<sup>2</sup>*Bonn-Cologne Graduate School of Physics and Astronomy, University of Bonn, Bonn, Germany*

<sup>3</sup>*Institute of Physics Belgrade, University of Belgrade, Serbia*

<sup>4</sup>*RWTH Aachen University, Aachen, Germany*

<sup>5</sup>*Institute for Theoretical Physics, University of Cologne, 50937 Köln, Germany*

Both natural and man-made supply networks exhibit universal structural patterns, such as the formation of loops. These patterns can be understood in terms of optimization models, assuming that biological networks evolved to optimal states and technical networks are designed to function optimally. In this article, we analyze networks that minimize dissipation under a resource constraint. We demonstrate spontaneous symmetry breaking in optimal network structures as a function of resource scaling. We show that fluctuations intricately impact the structure and can lead to a reentrant transition from a symmetry-broken state to a symmetric state and back again.

## I. INTRODUCTION

Supply networks are fundamental components of both natural and engineered systems. In nature, for instance, leaf venation networks distribute water and nutrients throughout plant tissues [1], while vascular networks deliver oxygen and nutrients to cells in vertebrate organisms [2, 3]. In human society, we rely on the function of infrastructure networks such as power grids [4], transportation networks [5], and hydraulic systems [6]. Additionally, networks shaped by long-term geological processes, such as river basins, often exhibit similar structural characteristics [7]. Identifying the physical principles that govern their organization remains a central challenge in network science [8].

Different structural patterns are found in supply networks across scientific disciplines. A prime example is the transition between radial and meshed networks [5, 9, 10]. Leaf venation networks are generally meshed [11] except for several old species such as Ginkgo [12]. Electric power grids are meshed on the high-voltage level, but radial on the low-voltage level [4]. It has been discussed that these universal structural patterns can be understood from optimization models, assuming that biological networks evolved to an optimal state [13–15] while technical networks are designed using optimization methods [16, 17]. That is, real-world supply networks typically minimize a characteristic property such as the dissipation or the necessary resources.

Symmetry is a key concept in statistical physics. A phase transition to an ordered phase is often accompanied by spontaneous symmetry breaking [18]: A physical system possesses certain symmetries which are broken in the ordered phase. For instance, the free energy is typically symmetric with respect to spatial rotations or translations, while its minimizer is not. Do these concepts equally apply to optimal supply networks across

disciplines? Recently, it has been shown that symmetry breaking occurs in large-scale simulation models of transportation networks [19].

In this article, we investigate symmetry breaking in a cornerstone model of optimal supply networks, which allows for comprehensive analytic insights [20, 21]. The model assumes a set of sources and sinks connected by a set of potential edges. The edge weights are optimized to minimize the dissipation subject to a resource constraint. This model has been shown to explain essential structural patterns of supply networks, such as the shape of leaf venation networks [13], the transition between radial and meshed networks [10, 22], or the emergence of community structures [23]. Randomness, either through fluctuating sources and sinks or through random failures, plays an essential role for the network structure [24].

Here, we examine situations in which the set of sources and sinks has discrete rotational symmetries. The key question is whether the optimal network structure retains this symmetry or if it is spontaneously broken. First, we consider elementary networks that allow for a comprehensive analytic characterization of the symmetry-breaking transition. Then, we extend our analysis to multilayer networks, which can be used to model interconnected, multi-energy networks. In this case, we focus on the symmetry of the respective layers. Randomness has a striking effect on the optimal network structure. We demonstrate a reentrant phase transition from a symmetry-broken phase to a symmetric phase and back again as the noise strength increases.

The article is organized as follows. We review the properties of linear flows networks and minimum dissipation network model in Sec. II. In Sec. III, we analyze symmetry breaking in ring networks with alternating sources and sinks. This model network allows for a semi-analytic treatment and thus provides a comprehensive analysis. In Sec. IV, we extend the analysis of randomness and investigate fluctuation that emerge in highly renewable energy systems. In Sec. V, we investigate the optimal structure of multilayer networks and demonstrate symmetry breaking between the layers and in the inter-layer

\* d.witthaut@fz-juelich.de

connections. We summarize and discuss our findings in Sec. VI.

## II. FUNDAMENTALS OF LINEAR AND OPTIMAL NETWORKS

### A. Linear flow networks

A flow network is modeled as a weighted graph  $G = (\mathcal{V}, \mathcal{E})$ , where the edges may describe pipes in a hydraulic network, veins in a biological supply network or transmission lines in an AC power grid. For each node  $n \in \mathcal{V}$ , there is an in- or outflow  $S_n$ , such that  $S_n > 0$  characterizes a source and  $S_n < 0$  a sink. We will always assume that the network is balanced such that  $\sum_n S_n = 0$ . In many applications, the flow  $F_{n \rightarrow m}$  over an edge is linear in the gradient of a potential,

$$F_{n \rightarrow m} = k_{nm}(\theta_n - \theta_m). \quad (1)$$

This linear relation holds, for instance, for hydraulic and vascular networks where the flow of water through a pipe or vein is proportional to the pressure drop [6, 13]. In high-voltage AC power grids, the flow of real power is approximately proportional to the difference of nodal voltage phase angles [4]. In DC electric circuits, Eq. (1) is just Ohm's law. The flows must satisfy the continuity equation or Kirchhoff's current law (KCL)

$$\sum_{m \in \mathcal{V}} F_{n \rightarrow m} = S_n \quad (2)$$

at every node  $n \in \mathcal{V}$ . If the injections  $S_n$  are given, the equations (1) and (2) completely determine the flows in the network. We remark that the injections can fluctuate over time such that the  $S_n$  must be treated as random variables.

For further analysis, we introduce a compact vectorial notation of the network equations. To this end, we label all edges consecutively as  $e = 1, \dots, |\mathcal{E}|$  and fix an orientation to keep track of the direction of the edge flows. Flows, injections and potentials are collected in the vectors  $\mathbf{F} = (F_1, \dots, F_{|\mathcal{E}|})^\top$ ,  $\mathbf{S} = (S_1, \dots, S_{|\mathcal{V}|})^\top$ , and  $\boldsymbol{\theta} = (\theta_1, \dots, \theta_{|\mathcal{V}|})^\top$ . The edge capacities are summarized in the diagonal matrix  $\mathbf{K} = \text{diag}(k_1, \dots, k_{|\mathcal{E}|})$ . For bookkeeping purposes, we define the node-edge incidence matrix  $\mathbf{E} \in \mathbb{R}^{|\mathcal{V}| \times |\mathcal{E}|}$  with components [25]

$$E_{n,e} = \begin{cases} 1 & \text{if edge } e \text{ starts at node } n, \\ -1 & \text{if edge } e \text{ ends at node } n, \\ 0 & \text{otherwise.} \end{cases} \quad (3)$$

Kirchhoff's current law (4) and Ohm's law (5) then read

$$\mathbf{S} = \mathbf{E}\mathbf{F} \quad (4)$$

$$\mathbf{F} = \mathbf{K}\mathbf{E}^\top \boldsymbol{\theta}. \quad (5)$$

We can solve these equations by substituting Ohm's law into Kirchhoff's law to obtain

$$\mathbf{S} = \underbrace{\mathbf{E}\mathbf{K}\mathbf{E}^\top}_{=: \mathbf{L}} \boldsymbol{\theta}. \quad (6)$$

where  $\mathbf{L}$  is the Laplacian of the network [25]. If the network is connected, then the Laplacian is of rank  $|\mathcal{V}| - 1$ . Nevertheless, we can solve equation (6) using the Moore-Penrose pseudoinverse  $\mathbf{L}^+$  as long as  $\sum_n S_n = 0$  and obtain

$$\boldsymbol{\theta} = \mathbf{L}^+ \mathbf{S} \quad \Rightarrow \quad \mathbf{F} = \mathbf{K}\mathbf{E}^\top \mathbf{L}^+ \mathbf{S}. \quad (7)$$

### B. Minimum dissipation networks

We consider a model of optimal supply networks introduced by Corson [10] and Katifori et al [13] extending previous models introduced in Refs. [20, 21]. The model is based on the observation that the linear flows (5) minimize the dissipation

$$D = \sum_{\substack{e \in \mathcal{E} \\ k_e > 0}} \frac{F_e^2}{k_e} \quad (8)$$

under the constraint  $\mathbf{S} = \mathbf{E}\mathbf{F}$  for every injection pattern  $\mathbf{S}$ . The optimal network model assumes that the edge capacities evolve such that the average dissipation

$$\bar{D} = \sum_{\substack{e \in \mathcal{E} \\ k_e > 0}} \frac{\langle F_e^2 \rangle}{k_e} \quad (9)$$

assumes a minimum. Here,  $\langle \cdot \rangle$  denotes the expected value taking into account the random fluctuations of the injection vector  $\mathbf{S}$ .

The overall resources are assumed to be limited, giving rise to the constraint

$$\sum_{e \in \mathcal{E}} k_e^\gamma \leq \kappa^\gamma. \quad (10)$$

where  $\kappa^\gamma > 0$  quantifies the available resources. Without loss of generality, we can assume that all possible resources are used to minimize the expected dissipation  $\bar{D}$ . Hence, we can replace the smaller equal sign with an equal sign, which simplifies calculations. The scaling parameter  $\gamma > 0$  depends on the type of problem under consideration. For example, Poiseuille flow through a cylindrical pipe of radius  $r_e$  and fixed length scales as  $F_e \sim r_e^4$ , while the circumference scales as  $r_e^2$ . Assuming that the mass of the pipe is limited, we obtain a resource constraint with a scaling exponent of  $\gamma = 1/2$ .

For a network with given capacities  $k_e$ , we can link the expected value of the dissipation  $\bar{D}$  to the injections  $S_n$  using the tools introduced in Sec. II A. Inserting the relation (7) into the expression (9), we obtain

$$\bar{D} = \sum_{e \in \mathcal{E}} k_e \sum_{i,j,n,m \in \mathcal{V}} E_{n,e} E_{m,e} (\mathbf{L}^+)_{n,i} (\mathbf{L}^+)_{m,j} \langle S_i S_j \rangle. \quad (11)$$

### C. Numerical Computation

In this article, we use analytically solvable models as well as numerical simulations to investigate symmetry breaking in optimal networks. Corson proposed a method for the numerical computation of optimal network structures based on self-consistency arguments [10]. The resource constraint is taken into account via the method of Lagrangian multipliers. For any local minimum, the gradient of the Lagrangian with respect to a  $k_e$  must vanish, resulting in the condition

$$\begin{aligned} & -\langle F_e^2 \rangle k_e^{-2} + \lambda \gamma k_e^{\gamma-1} = 0, \\ \Rightarrow \quad k_e &= \left( \frac{\langle F_e^2 \rangle}{\gamma \lambda} \right)^{1/(1+\gamma)} \end{aligned}$$

The Lagrangian multiplier  $\lambda$  is fixed by the resource constraint which yields

$$k_e = \frac{\langle F_e^2 \rangle^{1/(1+\gamma)}}{(\sum_{l \in \mathcal{E}} \langle F_l^2 \rangle^{\gamma/(1+\gamma)})^{1/\gamma}} \cdot \kappa \quad (12)$$

Then one can iteratively find a (local) minimum of the expected dissipation. Starting from an initial guess for the edge capacities  $k_e$ , one repeats the following steps until convergence,

1. For a given guess of the edge capacities  $k_e$ , compute the expected value  $\langle F_e^2 \rangle$  for each edge  $e \in \mathcal{E}$  using Eq. (11).
2. Update the edge capacities  $k_e$  via Eq. (12)
3. Compute that norm of the change of the edge capacities. If the norm drops below a certain threshold, stop the iteration.

In general, several local minima exist for a given set of edges  $\mathcal{E}$  and injections  $S_j$ . The algorithm will converge to one of these local minima depending on the initial guess.

## III. SYMMETRY BREAKING IN NETWORKS WITH RING GEOMETRY

### A. Model Network

We introduce a class of elementary networks to elucidate the main mechanisms of symmetry breaking in optimal networks. We consider two types of nodes, sources (generators) and sinks (consumers). Consequently, the vertex set is written as  $\mathcal{V} = \mathcal{V}_g \cup \mathcal{V}_c$  with  $N_g = |\mathcal{V}_g|$  and  $N_c = |\mathcal{V}_c|$ . We assume that the load at the sink nodes  $i \in \mathcal{V}_c$  is fixed as  $S_i = -\mu$ . The generation at the source nodes  $i \in \mathcal{V}_g$  fluctuates stochastically according to the law  $S_i = (N_c/N_g) \cdot \mu + X_i$ , where the  $X_i$  denote

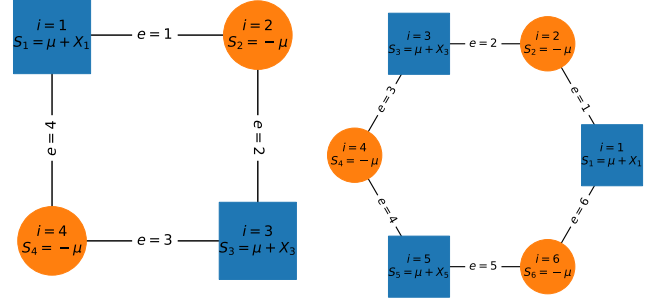


FIG. 1. Schematic of elementary ring networks for  $N = 2$  and  $N = 3$  with square generator nodes and circular consumer nodes.

identically distributed random variables with zero mean  $\langle X_i \rangle = 0$  and

$$\sum_{i \in \mathcal{V}_g} X_i = 0. \quad (13)$$

This condition assures that the network is always balanced, i.e. the aggregated generation matches the aggregated consumption. We note that such a distribution can be constructed from Dirichlet random variables. The statistics of the injections  $S_i$  enters the problem via the second moments, cf. Eq. (11). To quantify the strength of random fluctuations, we introduce the parameter

$$\beta^2 = -\langle X_i X_j \rangle \quad \text{for } i \neq j \in \mathcal{V}_g. \quad (14)$$

The second moments of the injections  $S_i$  are then given by (see appendix A for details)

$$\langle S_i S_j \rangle = \begin{cases} \frac{N_c^2}{N_g^2} \mu^2 + (N_g - 1) \beta^2 & i = j \in \mathcal{V}_g, \\ \frac{N_c^2}{N_g^2} \mu^2 - \beta^2 & \text{if } i \neq j \in \mathcal{V}_g, \\ \mu^2 & i, j \in \mathcal{V}_c \\ -\frac{N_c}{N_g} \mu^2 & i \in \mathcal{V}_g, j \in \mathcal{V}_c. \end{cases}$$

In this section we consider a ring network with adjacent source and sink nodes as shown in Fig. 1 for  $N_c = N_g = 2$  and  $N_c = N_g = 3$ . The vertices are labeled consecutively along the ring such that  $\mathcal{V}_g = \{1, 3, 5, \dots\}$  and  $\mathcal{V}_c = \{2, 4, 6, \dots\}$ . Edges link adjacent nodes with consecutive indices, i.e.  $e = (e, e + 1)$ .

For the given class of model networks, the optimization problem respects a discrete rotational symmetry

$$\begin{aligned} i &\rightarrow i' = i + 2, 4, 6, \dots \\ e &\rightarrow e' = e + 2, 4, 6, \dots \end{aligned}$$

Hence, the key question is whether the optimal capacities  $k_1, k_2, \dots$  respect this symmetry or whether symmetry is broken. In the following subsections we will demonstrate a phase transition between the symmetric and the symmetry-broken phase. The simplicity of the networks allows for an analytic treatment and thus sheds light on the mechanisms of symmetry breaking.

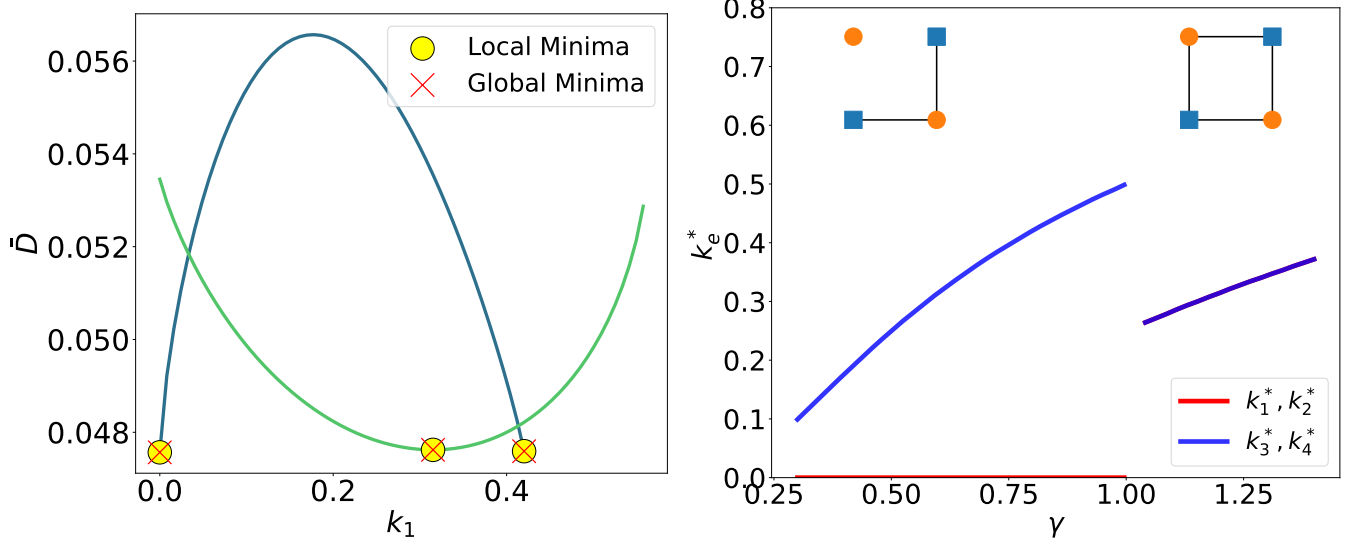


FIG. 2. Symmetry breaking via bifurcation in an elementary ring network with  $N = 2$ ,  $\mu = 0$  and  $\kappa = 1$ . Left: The expected dissipation  $\bar{D}(k_1)$  for two values of the scaling exponent  $\gamma$ , blue for  $\gamma = 0.8$  and green for  $\gamma = 1.2$ . For  $\gamma < 1$  there are two minima on the boundary of the domain corresponding to symmetry-broken states with  $k_1^* = k_2^* = 0$  and  $k_3 = k_4 = 2^{-\gamma}\kappa$  or  $k_3^* = k_4^* = 0$  and  $k_1 = k_2 = 2^{-\gamma}\kappa$ . For  $\gamma > 1$  there is a single local minimum corresponding to a symmetric state  $k_1^* = k_2^* = k_3^* = k_4^* = \kappa \cdot 4^{-1/\gamma}$ . Right: The optimal edge capacities as a function of the scaling exponent  $\gamma$ . The insets visualize the optimal network structure.

### B. Mechanisms of symmetry breaking

We first consider the basic case  $\mu = 0$  to analyze the basic routes to symmetry breaking. In this case, the injection  $S_i$  vanishes for all load nodes  $i \in \{2, 4, 6, \dots\}$ . Kirchhoff's current law then shows that the flows on the edges adjacent to the sink nodes must be equal,

$$F_e = F_{e+1}, \quad \text{for } e \in \{1, 3, 5, \dots\}$$

Using Eq. (12), we see that the optimal network capacities are also equal,

$$k_e^* = k_{e+1}^*, \quad \text{for } e \in \{1, 3, 5, \dots\}.$$

Thus, we have reduced the number of free optimization variables by one half.

Let us first analyze the case  $N = 2$  for which we obtain  $k_1 = k_2$  and  $k_3 = k_4$ . Using the resource constraint (10) in its equality form, we obtain

$$k_3 = \left( \frac{1}{2} \kappa^\gamma - k_1^\gamma \right)^{1/\gamma}, \quad (15)$$

such that we are left with a single optimization variable  $k_1 \in [0, \kappa \cdot 2^{-1/\gamma}]$ . Plotting the expected dissipation  $\bar{D}$  as a function of  $k_1$  (Fig. 2), we observe the following. For  $\gamma < 1$ , the function  $\bar{D}(k_1)$  has two global minima at the boundary of the domain. The optimal network is symmetry-broken with either  $k_1 = k_2 = 0$ ,  $k_3 = k_4 = 2^{-\gamma}\kappa$  or  $k_3 = k_4 = 0$ ,  $k_1 = k_2 = 2^{-\gamma}\kappa$ . For  $\gamma > 1$ , the function  $\bar{D}(k_1)$  has a single minimum at

$k_1^* = 2^{-1/\gamma}\kappa$ . The optimal network is symmetric with  $k_1 = k_2 = k_3 = k_4 = 4^{-1/\gamma}\kappa$ . The transition between the two phases at  $\gamma_c = 1$  is discontinuous in the sense that the optimal edge capacities  $k_e^*$  jump discontinuously. We remark that discontinuity is a general feature of transitions in optimal networks as discussed in Ref. [22]. Moreover, the transition is associated with a bifurcation: the local minima vanish when  $\gamma$  crosses the critical value  $\gamma_c = 1$ . Note that it is possible to set  $\kappa = 1$  without loss of generality, as we have done in Fig. 2.

Next, we analyze the case  $N = 3$ . We can exploit Kirchhoff's current law again to show that  $k_1 = k_2$ ,  $k_3 = k_4$  and  $k_5 = k_6$ . Using the resource constraint (10) we can further eliminate one optimization variable and obtain

$$k_5 = \left( \frac{1}{2} \kappa^\gamma - k_1^\gamma - k_3^\gamma \right)^{1/\gamma}, \quad (16)$$

Thus, we are left with two optimization variables,  $k_1$  and  $k_3$ . Plotting the expected dissipation  $\bar{D}$  as a function of  $k_1$  and  $k_3$  (Fig. 3), we observe the following. For  $\gamma = 0.55$ , the expected dissipation  $\bar{D}(k_1, k_3)$  assumes its global minimum for a symmetry-broken state where either  $k_1 = 0$ ,  $k_3 = 0$  or  $k_5 = 0$ . The symmetric state  $k_1 = k_3 = k_5$  is a local minimum, but the expected dissipation  $\bar{D}$  is larger than at the global minimum. For  $\gamma = 0.6$ , both the symmetric and the symmetry-broken states remain local minima, but the global minimum changes. Now,  $\bar{D}$  is lower for the symmetric states than for the symmetry-broken states. We thus observe a transition between a symmetry-broken phase for  $\gamma$  below a critical value  $\gamma_c$ , and a symmetric phase for  $\gamma$  above the

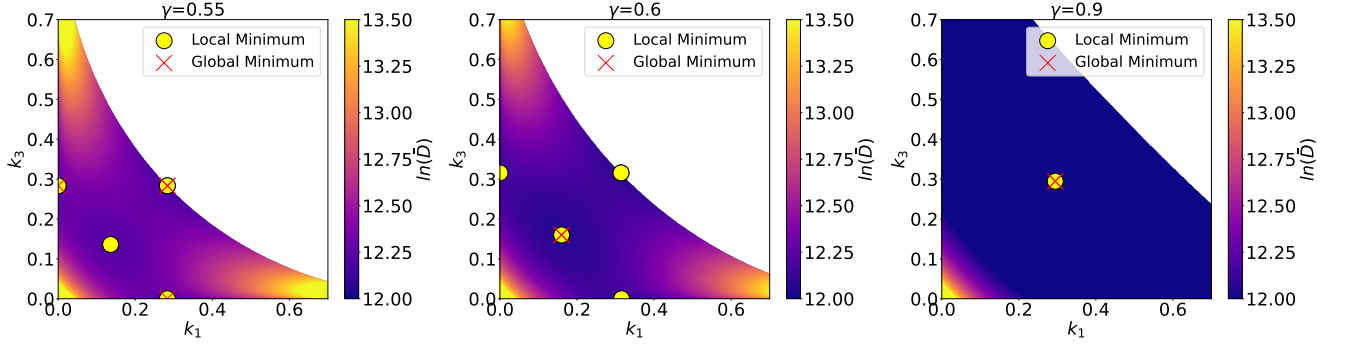


FIG. 3. Symmetry breaking via an exchange of local and global minima in an elementary ring network with  $N = 3$  and  $\mu = 0$ . The figures show the expected dissipation  $\bar{D}(k_1, k_3)$  for three values of the scaling exponent  $\gamma$ . For  $\gamma = 0.55$  there are three minima on the boundary of the domain corresponding to symmetry-broken states. The symmetric state is a local minimum but has a higher value of  $\bar{D}$ . For the value of the expected dissipation  $\bar{D}$  is higher than for the symmetry-broken state. For  $\gamma = 0.8$  the minima exchange roles: The symmetric state is the global minimum while the symmetry-broken states are local minima with a higher value of the dissipation. No local minimum is lost during the transition to symmetry breaking.

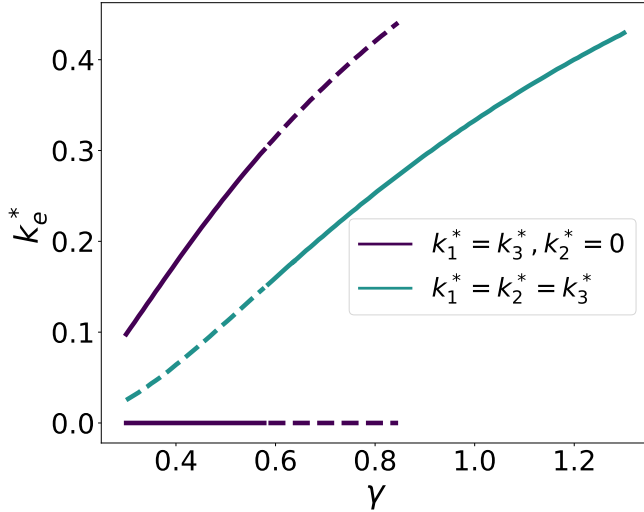


FIG. 4. The optimal edge capacities as a function of the scaling exponent  $\gamma$  in an elementary ring network with  $N = 3$  and  $\mu = 0$ . The solid lines correspond to global minima and the dashed lines correspond to local minima. The symmetry-breaking transition takes place at a critical value  $\gamma_c$  depicted by an exchange of roles of the local and global minima, while the local minima undergo a bifurcation and vanish at a different value  $\gamma_b$ .

critical value  $\gamma_c$ . The transition is discontinuous as the optimal values of the edge capacities  $k_e^*$  jump discontinuously. However, the transition is not associated with a bifurcation of local minima as in the case  $N = 2$ , since none of them vanish.

We further note that the symmetry-broken local minima vanish when  $\gamma$  exceeds a threshold  $\gamma_b \approx 0.85$  (Fig. 3c and Fig. 4). That is, there is still bifurcation of local minima but it does not coincide with the symmetry breaking transition.

We summarize our findings so far. We have demon-

strated a symmetry breaking phase transition in minimum dissipation networks when the scaling exponent crosses a critical value  $\gamma_c$ . The transition is generally discontinuous in the sense that the optimal edge capacities  $k_e^*$  jump at the transition point. Two basic mechanisms are possible: First, the transition may be associated with a bifurcation where one local minimum vanishes and another one occurs if  $\gamma$  crosses  $\gamma_c$ . Second, the transition may occur when a global and a local minima exchange roles, but no local minimum is lost.

### C. The phase diagram of symmetry breaking

We now turn back to the full model and construct the phase diagram of the optimal dissipation networks. We fix  $\mu = 1$  and focus on the impact of fluctuations quantified by the parameter  $\beta$ .

We proceed as follows. For every value of the parameters  $\gamma$  and  $\beta$ , we compute the expected dissipation  $\bar{D}$  for a symmetric and a symmetry-broken configuration

$$\begin{aligned} \text{symmetric: } k_1 = k_2 = \dots = k_{2N} &= (2N)^{-\frac{1}{\gamma}} \kappa \\ \text{symmetry-broken: } k_{2N} &= 0. \end{aligned} \quad (17)$$

The computation can be carried out partly analytically as outlined in appendix B. Furthermore, we use the numerical scheme described in Sec. II C with different initial guesses to validate the semi-analytic results. We use (i) the symmetric and symmetry-broken configurations to check whether these state are local minima and (ii) random initial guesses to exclude that a different global minimum exists.

The results of our analysis are shown in (Fig. 5). We plot the minimum edge capacity  $\min_{e \in \mathcal{E}} k_e$  to distinguish between the symmetry-broken phase with  $\min_{e \in \mathcal{E}} k_e = 0$  and the symmetric phase with  $\min_{e \in \mathcal{E}} k_e > 0$ . For a fixed value of the fluctuation parameter  $\beta$ , we find a

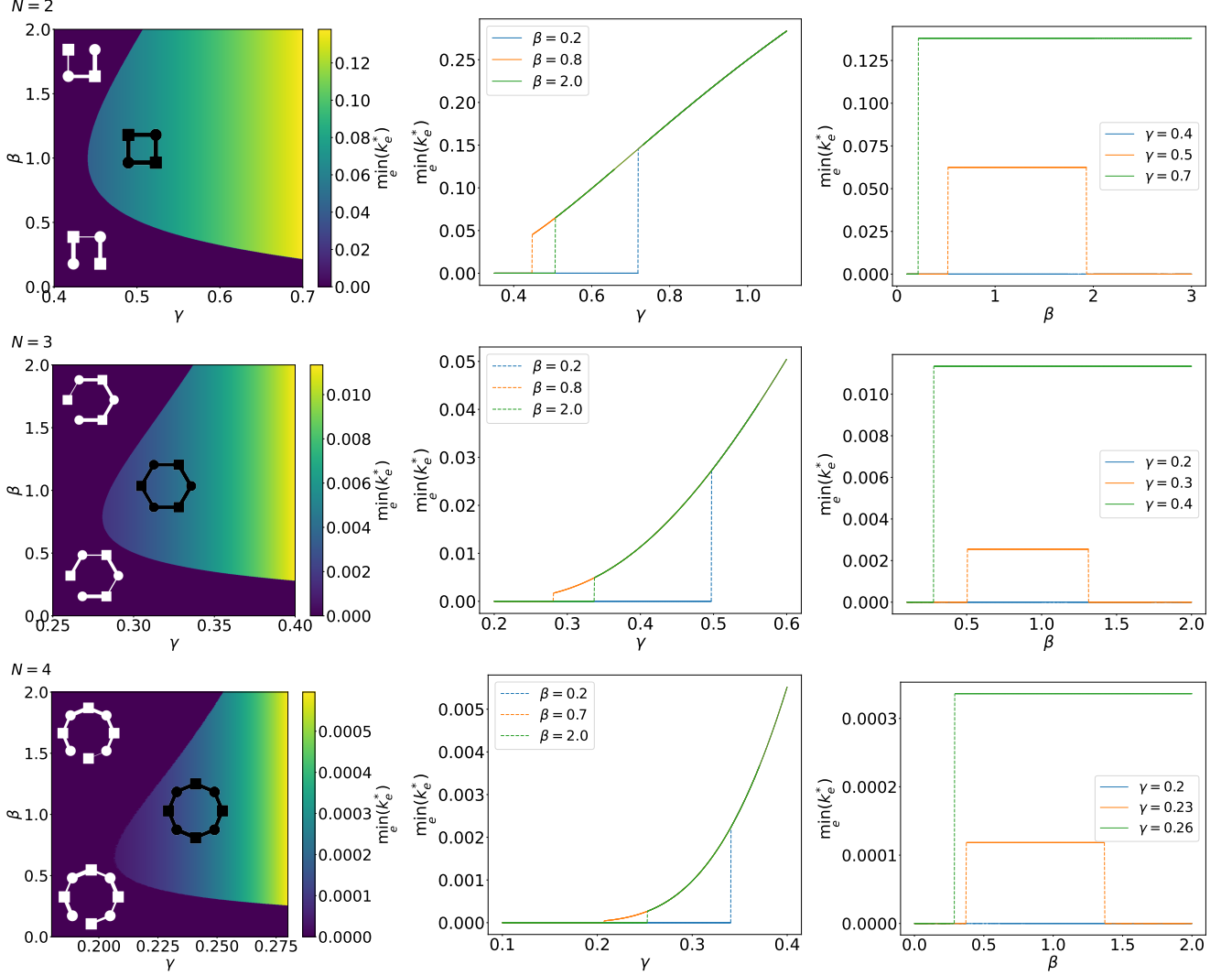


FIG. 5. Phase diagram of the optimal network structure for the model class shown in Fig. 1. We plot the smallest edge capacity in the optimal network  $\min_{e \in \mathcal{E}} k_e^*$  as a function of the fluctuation strength  $\beta$  and the scaling exponent  $\gamma$  for  $N = 2$  (top),  $N = 3$  (middle) and  $N = 4$  (bottom). Symmetry breaking is indicated by  $\min_{e \in \mathcal{E}} k_e^* = 0$ , i.e. one edge is missing in the optimal networks. Left: Phase diagram as a function of  $\beta$  and  $\gamma$ . The insets visualize the optimal network structure in the corresponding regions. Middle: Optimal network state as a function of the scaling exponent  $\gamma$ . The optimal state changes discontinuously from symmetry-broken to symmetric when  $\gamma$  exceeds a critical value  $\gamma_c$ . We find  $\gamma_c < 1$  unless fluctuations vanish entirely. Right: Optimal network state as a function of the fluctuation strength  $\beta$ . For intermediate values of  $\gamma$  we find a reentrant phase transition from symmetry-broken to symmetric and back.

transition from a symmetry-broken phase to a symmetric phase when the scaling exponent  $\gamma$  increases. The critical value satisfies  $\gamma_c \leq 1$ , where equality holds only for  $\beta = 0$ . That is, the phase transition generally occurs for  $\gamma_c < 1$  in a system with non-vanishing fluctuations. The transition is always discontinuous as discussed for the elementary examples in Sec. III B.

A remarkable behavior is observed when we monitor the optimal network as a function of the fluctuation parameter  $\beta$ . For certain values of  $\gamma$  we find a reentrant phase transition from the symmetry-broken phase to the symmetric phase and back to the symmetry-broken phase. Hence, more fluctuations do not always favor

more connectivity.

The reentrant behavior can be deduced from the scaling behavior of the expected dissipation in the symmetry-broken state  $\bar{D}_a$  and the symmetric state  $\bar{D}_s$  (Fig. 6). For large values of  $\beta$  we find the scaling

$$\bar{D}_s \sim \beta^{1.61}, \quad \text{and} \quad \bar{D}_a \sim \beta^{1.40}. \quad (18)$$

That is the expected dissipation  $\bar{D}_s$  grows faster as  $\bar{D}_a$  such that the symmetry-broken network is optimal. For banishing fluctuations, the expected dissipation  $\bar{D}_s$  levels off at a value of

$$\bar{D}_s(\beta = 0) = 6.86, \quad \text{and} \quad \bar{D}_a(\beta = 0) = 4.44. \quad (19)$$



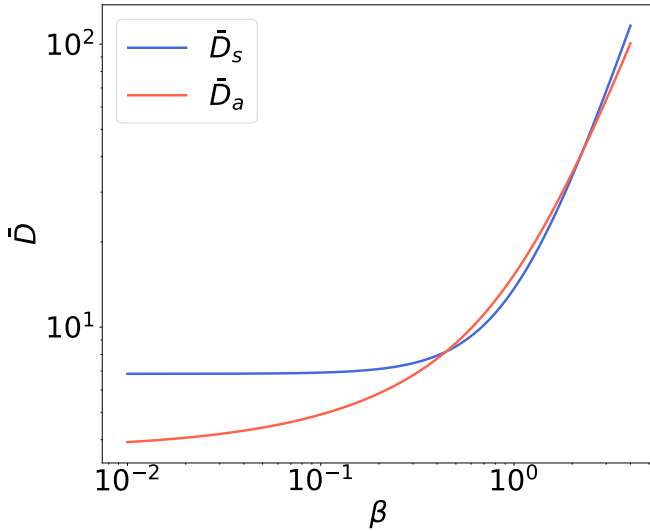


FIG. 6. Scaling behavior of the expected dissipation in the symmetry-broken state  $\bar{D}_a$  and the symmetric state  $\bar{D}_s$  with the fluctuation strength  $\beta$ . Results are shown for  $N = 2$  and  $\gamma = 0.53$ .

such that the symmetry-broken network is also optimal in this parameter region. Only for intermediate values of  $\beta$  we find  $\bar{D}_a > \bar{D}_s$  such that the optimal network is symmetric.

A qualitative explanation is provided by the structure of the optimal networks sketched in Fig. 5. We observe that optimal symmetry-broken networks for small and large  $\beta$  differ considerably. For small  $\beta$ , sources and sinks balance locally. That is, every source can supply one adjacent sink up to small residual fluctuations. Hence, the optimal network contains  $N$  strong edges linking one source and one sink each. For large  $\beta$ , fluctuations between the sources become dominant. Global balancing between the source nodes necessitates an extended backbone of strong edges. For intermediate values of  $\beta$ , symmetric networks are favorable even for small values of  $\gamma$  because they enable both local and global balancing.

#### D. Scaling with system size

We now analyze how the critical behavior scales with system size. We consider the smallest value of  $\gamma$  for which the transition from the symmetry-broken to symmetric state occurs. This is the cusp point in the phase diagrams in Figure 5, i.e. the smallest  $\gamma$  for which  $\min_{e \in \mathcal{E}} k_e > 0$ . We can find  $\gamma_c$  theoretically, since the average dissipation for the symmetric and symmetry-broken states,  $\bar{D}_s$  and  $\bar{D}_a$  can be obtained semi-analytically, as described in Appendix B. Then we can numerically determine the smallest  $\gamma$  value for which the curves  $\bar{D}_s(\beta)$  and  $\bar{D}_a(\beta)$  cross. Repeating this procedure for a range of  $N \in [2, 9]$  values reveals a power law

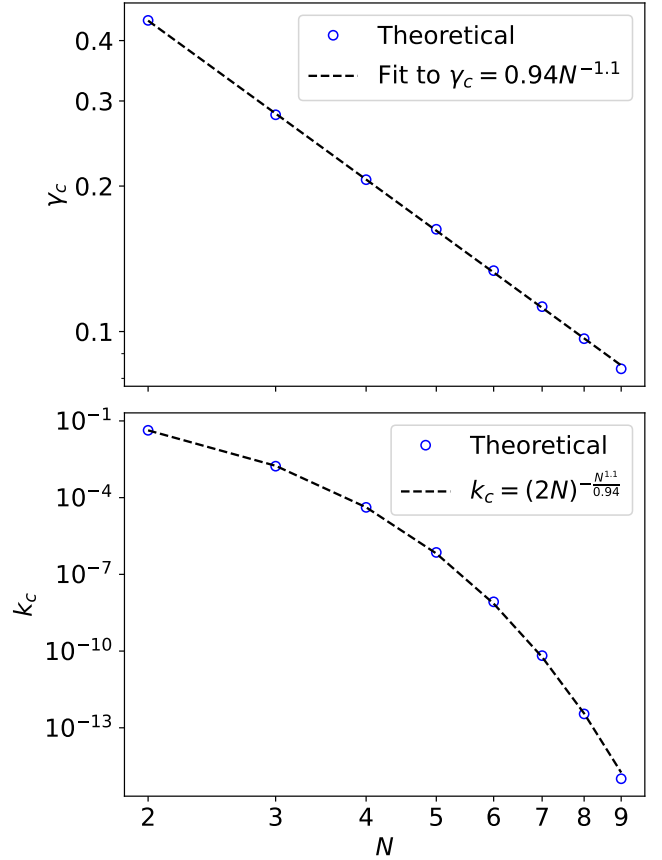


FIG. 7. Scaling with system size  $N$  of the minimal value  $\gamma_c$  for which we observe the phase transition between symmetry-broken and symmetric states (top), and the corresponding symmetrical capacity values  $k_c$  (bottom). We fit the theoretical values from the top panel to  $\gamma_c = cN^{-\alpha}$  using nonlinear least squares. In the bottom panel, we keep the constants from the previous fit.

dependence of the critical value on the system size

$$\gamma_c \sim cN^{-\alpha}$$

as shown in the top panel of Fig. 7. We apply the nonlinear least squares method to obtain the scaling exponent  $\alpha$  and constant factor  $c$ ,

$$\alpha = 1.092 \pm 0.004$$

$$c = 0.938 \pm 0.004.$$

Using this result, we can quantify the discontinuity of the symmetry breaking phase transition at  $\gamma_c$  as a function of the system size. In the symmetrical phase, all capacities are equal to  $k = (2N)^{-\frac{1}{\gamma}}$  according to Eq. (17). Hence, the corresponding edge capacities at the cusp point will have a super-exponential dependence on  $N$ ,

$$k_c = (2N)^{-\frac{N^\alpha}{c}}.$$

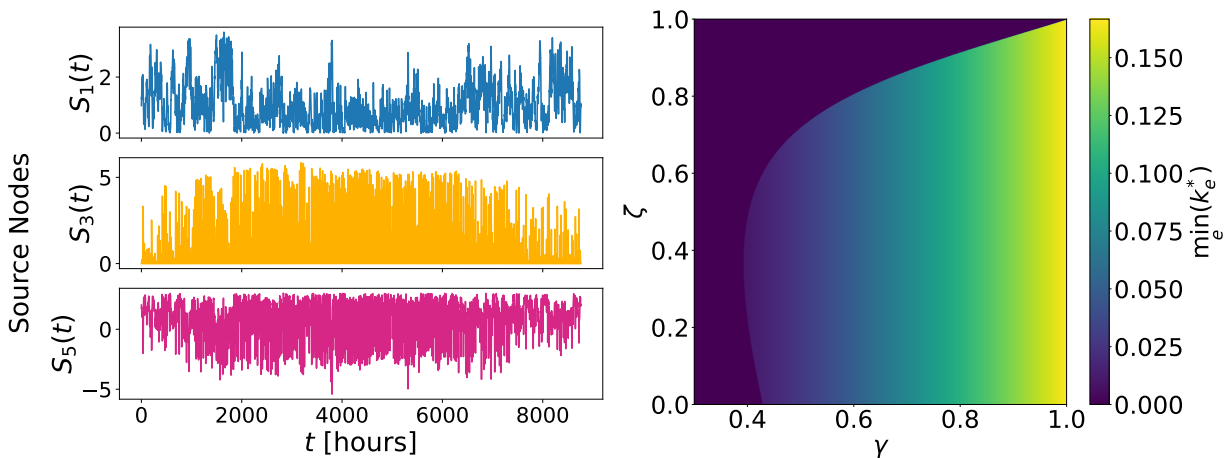


FIG. 8. Symmetry breaking in a network with fluctuating generation by renewable power sources. Left: Fluctuating generation of wind turbines  $Z_1(t)$ , solar photovoltaics  $Z_3(t)$  and backup power plants  $Z_5(t)$ . Right: Phase diagram of the optimal network structure as a function of the scaling exponent  $\gamma$  and the share of fluctuating renewable power  $\zeta$ . We assume a ring network with six nodes as sketched in Fig. 1 with fluctuating generators  $S_i(t) = (1 - \zeta)\mu + \zeta Z_i(t)$ .

In the lower panel of Figure 7, we demonstrate that the previously obtained fitting coefficients accurately describe the behavior of  $k_c$  as a function of  $N$ . Consider now the minimum edge capacity  $\min_e k_e^*$  as in the phase diagrams in Fig. 5. At the cusp, this quantity jumps from zero to  $k_c$ . Hence, the symmetry-breaking phase transition is always discontinuous, but the discontinuity decreases rapidly with the system size.

#### IV. SYMMETRY BREAKING IN ENERGY GRIDS

The current model for symmetry breaking in optimal networks crucially relies on the existence of anti-correlations between the generations  $S_i$ . We argue that such a situation routinely occurs in energy systems such that symmetry breaking is relevant in the design of optimal energy grids.

We consider a network that is similar to the ones shown in Fig. 1 with  $N = 3$  where every node corresponds to a geographical region. Regions  $i = 2, 4, 6$  consume power such that the injection can be written as  $S_i = -\mu$ . We assume that region  $i = 1$  features wind turbines and region  $i = 3$  features solar photovoltaic plants, such that power generation at a time  $t$  can be written as

$$S_1(t) = (1 - \zeta)\mu + \zeta\mu Z_1(t), \quad (20)$$

$$S_3(t) = (1 - \zeta)\mu + \zeta\mu Z_3(t), \quad (21)$$

where  $Z_1$  and  $Z_3$  denote the normalized capacity factors of a wind turbine or solar PV plant and the parameter  $\zeta \in [0, 1]$  measures the share of fluctuating renewable power generation. The capacity factor is defined as the ratio of the actual power generation at time  $t$  divided by the maximum generation. Here, we rescale the capacity factor by a constant number such

that  $\langle Z_1 \rangle = 1 = \langle Z_3 \rangle$ . Finally, we assume that region 5 hosts storage infrastructures that provide or consume the power  $S_5(t) = 3\mu - S_1(t) - S_3(t)$ . For our numerical experiment we use time series obtained from renewables.ninja [26, 27] for the year 2019 at the location Jülich. The second moments are then computed via the empirical time average

$$\langle S_i S_j \rangle = \frac{1}{T} \sum_{t=1}^T S_i(t) S_j(t), \quad (22)$$

where  $T$  denotes the number of time steps in the data. The three random variables  $S_1, S_3, S_5$  are strongly anti-correlated. The anti-correlation of wind and solar power generation is mostly due to seasonal effects, solar power being stronger in the summer and wind power stronger in the winter [28]. Backup plants are primarily used when neither wind or solar power is available, which also introduces strong anti-correlations.

The resulting phase diagram of the optimal network structure is shown in Fig. 8 on the right. Depending on the cost parameter  $\gamma$  and the fluctuation strength  $\zeta$ , the optimal network is either an open ring with  $\min_e k_e^* = 0$  or a closed ring with  $\min_e k_e^* > 0$ . The overall shape of phase diagram is very similar to the ones studied in Fig. 5: A closed ring is found if the cost parameter  $\gamma$  exceeds a threshold. Remarkably, we again find a reentrant behavior in terms of the fluctuation strength  $\zeta$  for intermediate values of  $\gamma$ .

We remark that this setup is no longer fully symmetric as the generation variables  $S_1, S_3$  and  $S_5$  no longer have an identical distribution. Nevertheless, the phase transition is largely analogous to the symmetry-breaking transition studied so far as the optimal network changes discontinuously from an open to a closed loop.



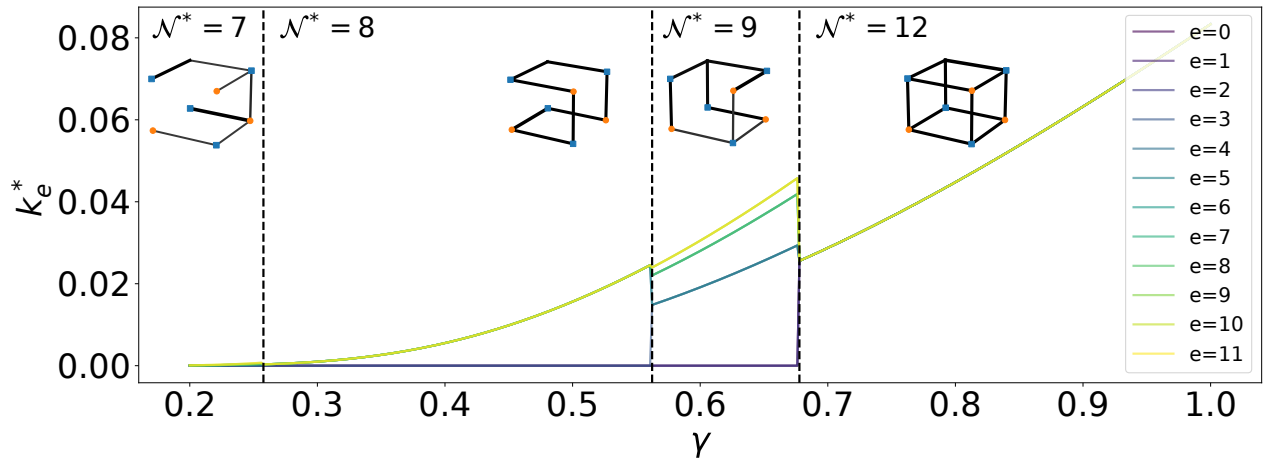


FIG. 9. Edge capacities  $k_e^*$  in elementary multiplex networks for  $\mu = 1$  and  $\beta = 0.5$ , for  $e = 0, 2, \dots, 11$ .  $\mathcal{N}^*$  denotes the number of nonzero edges in the network, such that vertical black dashed lines separate regimes with different edge numbers. Insets show examples of optimal network structures for  $\gamma = 0.2$ ,  $\gamma = 0.4$ ,  $\gamma = 0.6$ , and  $\gamma = 0.8$  (left to right), whereby the line width is proportional to the optimal edge capacities  $k_e^*/\max_e(k_e^*)$ .

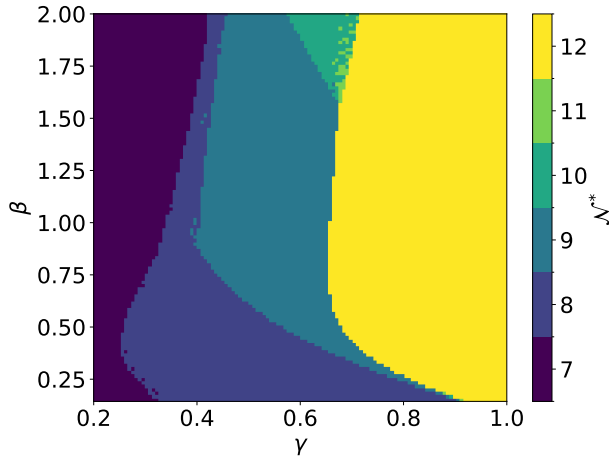


FIG. 10. Phase diagram of the optimum structure for a cube network (cf. Fig. 9). We show the number  $\mathcal{N}^*$  of edges with nonvanishing capacity  $k_e > 0$  as a function of the cost parameter  $\gamma$  and the noise strength  $\beta$ .

## V. SYMMETRY BREAKING IN MULTILAYER NETWORKS

In this section we extend our analysis to multilayer networks. In the context of energy grids, the different layers might correspond to different energy carriers while inter-layer connections correspond to conversion systems [29]. The design of such multi-energy system crucially depends on the fluctuations of generation and demand [30]. A key question is whether both layers are utilized and connected symmetrically.

We begin our analysis with an elementary model network. We consider a three-dimensional (3D) cube with four sink nodes and four source nodes, whose gener-

ation fluctuates according to the model introduced in Sec. III A. This setup is symmetric with respect to a  $180^\circ$  rotation around the three axes passing through adjacent faces of the cube.

Figure 9 shows the optimal network structure as a function of the cost parameter  $\gamma$  for a comparably weak noise amplitude  $\beta = 0.5$ . The minimum dissipation network is fully symmetric for large values of  $\gamma$ . That is, all 12 edges of the cube have the same capacity  $k_e$ . As the value of  $\gamma$  decreases, redundant connections are suppressed [10]. Consequently, symmetry is spontaneously broken for  $\gamma \leq 0.66$ : The optimum network contains fewer than 12 edges with non-vanishing capacity  $k_e > 0$ . Interestingly, we observe a phase with  $\mathcal{N}^* = 8$  edges and partially conserved symmetry for intermediate values of  $\gamma$ . In this phase, the network is symmetric with respect to one axis but asymmetric with respect to the remaining two. Ultimately, the optimal network becomes a tree for very small values of the cost parameter,  $\gamma \leq 0.26$ .

The phase diagram in Fig. 10 summarizes how the optimum network structure depends on the cost parameter  $\gamma$  and the noise strength  $\beta$ . Once again we observe a reentrant behavior in the symmetry breaking phase transition. As  $\beta$  increases for  $\gamma \approx 0.7$ , the optimum network changes from symmetry-broken to symmetric and back to symmetry-broken. Notably, the partially symmetry-broken phase dominates for weak noise but is suppressed for strong noise.

We will now turn to extended multiplex networks. For the sake of simplicity we consider a network with two layers, each consisting of a finite square lattice with two sources (see Fig. 11). The two layers are connected by edges between all pairs of vertices in the same position in their respective lattices. As with the cube network studied above, the optimization problem is invariant under a  $180^\circ$  rotation around any of the three axes. Notably,

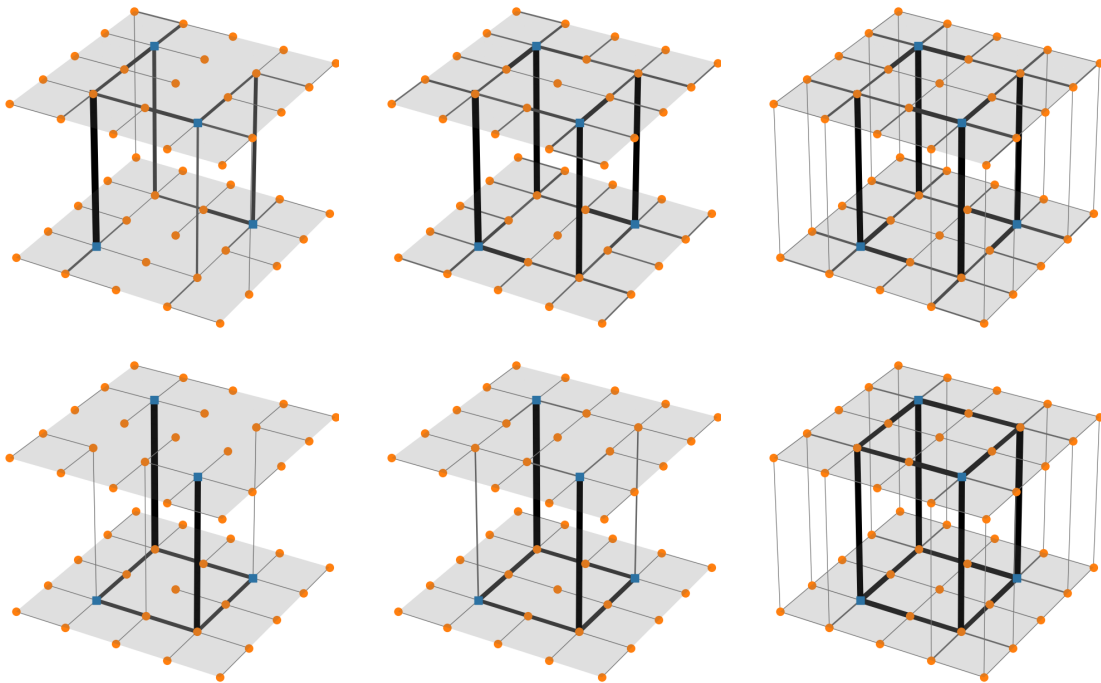


FIG. 11. Symmetry breaking in a multiplex network. We show the network structures that minimize the dissipation in a network with four sources (■) for (a-c) weak fluctuations  $\beta = 0.5$  and (d-f) strong fluctuations  $\beta = 2.0$ . The cost parameter increases from left to right.

a rotation around the  $z$ -axis maps the two layers onto themselves, while a rotation around the  $x$ - and  $y$ -axes exchanges them.

In the case of weak fluctuations, a source node typically supplies its neighboring sinks. Hence, the largest squared flows  $\langle F_e^2 \rangle$ , and thus the largest capacities  $k_e$ , are generally found for the edges  $e$  adjacent to the source nodes. Therefore, there are four strong edges connecting the two layers. For large values of the cost parameter  $\gamma$ , these four interlayer edges have the same capacity  $k_e$  respecting the symmetry of the optimization problem. This symmetry is spontaneously broken when  $\gamma$  decreases. Instead, the network becomes ultra-sparse.

A different manifestation of symmetry breaking is observed in the case of strong fluctuations ( $\beta = 2.0$ ). These fluctuations are balanced by strong flows between the source nodes. Hence, the squared flows  $\langle F_e^2 \rangle$  and the capacities  $k_e$  are large for edges  $e$  linking the four source nodes. For large values of the cost parameter  $\gamma$ , these strong edges form a cube, respecting the discrete rotational symmetry of optimization problem. In particular, a square of strong edges is observed in both layers of the network. As the cost parameter decreases, redundant connections become less likely [10]. Consequently, the symmetry between the two layers is spontaneously broken for  $\gamma \leq 0.7$ : Only one layer contains a square of strong edges. Two strong edges connect this ring to sources in the other layer.

## VI. CONCLUSION AND OUTLOOK

We demonstrated that symmetry breaking is a generic and robust feature of optimal supply networks under resource constraints and fluctuating demands. Using analytically tractable ring geometries and multi-layer network structures, we revealed the role of cost scaling, randomness, and network topology in driving spontaneous symmetry breaking in a classic model of dissipation-minimizing flows. Specifically, we identified discontinuous phase transitions separating symmetric and symmetry-broken network configurations and observed phenomena such as reentrant symmetry breaking induced by noise.

These results offer a new perspective on the structural patterns observed in natural and engineered supply networks. They suggest that asymmetric network structures can emerge from optimality principles alone, independent of explicit asymmetries in the problem formulation. Notably, we demonstrated that anticorrelated fluctuations, such as those in renewable energy systems, naturally lead to symmetry-broken network configurations. This highlights the practical relevance of our findings for designing robust and efficient infrastructure, particularly in contexts where variability and intermittency are key factors.

Our work opens several promising avenues for future research. On the theoretical side, a systematic classification of symmetry-breaking mechanisms across more general network topologies would deepen our understanding

of optimal network morphogenesis. On the applied side, integrating time-dependent operational constraints and nonlinear flow laws could further enhance the relevance of these models to real-world systems, ranging from vascular transport to smart grids. Lastly, the discovery of reentrant transitions suggests that fluctuations can both stabilize and destabilize symmetry — an insight that may inspire new design principles for adaptive and resilient networked systems.

### Appendix A: Second moments

In this appendix, we derive the second moments for the class of model networks introduced in section III A. For sink nodes  $i, j \in \mathcal{V}_g$  we have  $S_i = S_j = -\mu$  and thus

$$\langle S_i S_j \rangle = \mu^2.$$

For a source node  $i \in \mathcal{V}_g$  and a sink node  $j \in \mathcal{V}_c$  we obtain

$$\begin{aligned} \langle S_i S_j \rangle &= \left\langle \left( \frac{N_c}{N_g} \mu + X_i \right) (-\mu) \right\rangle \\ &= -\frac{N_c^2}{N_g^2} \mu^2 \end{aligned}$$

using  $\langle X_i \rangle = 0$ . For two different source nodes  $i \neq j \in \mathcal{V}_g$  we obtain

$$\begin{aligned} \langle S_i S_j \rangle &= \left\langle \left( \frac{N_c}{N_g} \mu + X_i \right) \left( \frac{N_c}{N_g} \mu + X_j \right) \right\rangle \\ &= +\frac{N_c^2}{N_g^2} \mu^2 + \langle X_i X_j \rangle \\ &= +\frac{N_c^2}{N_g^2} \mu^2 - \beta^2. \end{aligned}$$

Finally, we use the fact that generation and consumption are always balanced such that we obtain for  $i \in \mathcal{V}_g$ :

$$\begin{aligned} X_i &= -\sum_{\substack{j \in \mathcal{V}_g \\ j \neq i}} X_j \\ \implies \langle X_i^2 \rangle &= -\sum_{\substack{j \in \mathcal{V}_g \\ j \neq i}} \langle X_i X_j \rangle \\ &= +(N_g - 1)\beta^2. \end{aligned}$$

Hence we obtain for  $i \in \mathcal{V}_g$ :

$$\begin{aligned} \langle S_i S_i \rangle &= \left\langle \left( \frac{N_c}{N_g} \mu + X_i \right) \left( \frac{N_c}{N_g} \mu + X_i \right) \right\rangle \\ &= \frac{N_c^2}{N_g^2} \mu^2 + \langle X_i X_i \rangle \\ &= \frac{N_c^2}{N_g^2} \mu^2 + (N_g - 1)\beta^2 \end{aligned}$$

### Appendix B: Dissipation in the symmetric and symmetry-broken state

In this appendix we describe how to compute the expected dissipation  $\bar{D}$  for the symmetric and symmetry-broken states in the model networks analyzed in Sec. III. In the symmetric state we have

$$k_1 = k_2 = k_3 = k_4 = \dots = \kappa \cdot (2N)^{-1/\gamma} \quad (\text{B1})$$

such that the graph Laplacian can be written as

$$\begin{aligned} \mathbf{L} &= k_1 \tilde{\mathbf{L}} \\ \tilde{\mathbf{L}} &= \begin{pmatrix} +2 & -1 & 0 & 0 & 0 & \dots & -1 \\ -1 & +2 & -1 & 0 & 0 & \dots & 0 \\ 0 & -1 & +2 & -1 & 0 & \dots & 0 \\ \vdots & \vdots & \vdots & \vdots & \vdots & & \vdots \end{pmatrix}. \end{aligned}$$

Substituting this result into Eq. (11), we obtain

$$\begin{aligned} \bar{D}_s &= \frac{(2N)^{1/\gamma}}{\kappa} \sum_{e \in \mathcal{E}} E_{n,e} E_{m,e} \\ &\quad \times \sum_{i,j,n,m \in \mathcal{V}} \left( \tilde{\mathbf{L}}^+ \right)_{n,i} \left( \tilde{\mathbf{L}}^+ \right)_{m,j} \langle S_i S_j \rangle. \end{aligned}$$

Notably, the summed expression depends only on the system size  $N$  and fluctuation strength  $\beta$ . The dependence on the edge capacities and the scaling exponent  $\gamma$  is absorbed in the prefactor.

For symmetry-broken state we assume that  $k_{2N} = 0$ . The edge flows are determined by Kirchhoff's current law independently of the edge capacities,

$$\begin{aligned} F_e &= \sum_{i=1}^e S_i \\ \implies \langle F_e^2 \rangle &= \sum_{i,j=1}^e \langle S_i S_j \rangle. \end{aligned}$$

The optimal edge capacities are given by Eq. (12) and the expected dissipation by Eq. (11).

---

[1] L. Sack and C. Scoffoni, Leaf venation: structure, function, development, evolution, ecology and applications in the past, present and future, *New Phytologist* **198**, 983

(2013).

[2] R. N. Pittman, *Regulation of Tissue Oxygenation* (Morgan & Claypool Life Sciences, San Rafael, CA, 2011).

- [3] J. B. Kirkegaard and K. Sneppen, Optimal transport flows for distributed production networks, *Physical Review Letters* **124**, 208101 (2020).
- [4] D. Witthaut, F. Hellmann, J. Kurths, S. Kettemann, H. Meyer-Ortmanns, and M. Timme, Collective nonlinear dynamics and self-organization in decentralized power grids, *Reviews of modern physics* **94**, 015005 (2022).
- [5] A. A. Ganin, M. Kitsak, D. Marchese, J. M. Keisler, T. Seager, and I. Linkov, Resilience and efficiency in transportation networks, *Science advances* **3**, e1701079 (2017).
- [6] R. J. Houghtalen, A. Osman, and N. H. Hwang, *Fundamentals of hydraulic engineering systems* (Pearson London, 2016).
- [7] A. Konkol, J. Schwenk, E. Katifori, and J. B. Shaw, Interplay of river and tidal forcings promotes loops in coastal channel networks, *Geophysical Research Letters* **49**, e2022GL098284 (2022).
- [8] S. Havlin, D. Y. Kenett, E. Ben-Jacob, A. Bunde, R. Cohen, H. Hermann, J. W. Kantelhardt, J. Kertész, S. Kirkpatrick, J. Kurths, J. Portugali, and S. Solomon, Challenges in network science: Applications to infrastructures, climate, social systems and economics, *Eur. Phys. J. Spec. Top.* **214**, 273 (2012).
- [9] J. R. Banavar, F. Colaiori, A. Flammini, A. Maritan, and A. Rinaldo, Topology of the fittest transportation network, *Physical Review Letters* **84**, 4745 (2000).
- [10] F. Corson, Fluctuations and redundancy in optimal transport networks, *Physical Review Letters* **104**, 048703 (2010).
- [11] H. Ronellenfitsch, J. Lasser, D. C. Daly, and E. Katifori, Topological phenotypes constitute a new dimension in the phenotypic space of leaf venation networks, *PLoS computational biology* **11**, e1004680 (2015).
- [12] M. R. Carvalho, R. Turgeon, T. Owens, and K. J. Niklas, The hydraulic architecture of ginkgo leaves, *American Journal of Botany* **104**, 1285 (2017).
- [13] E. Katifori, G. J. Szöllősi, and M. O. Magnasco, Damage and fluctuations induce loops in optimal transport networks, *Physical review letters* **104**, 048704 (2010).
- [14] H. Ronellenfitsch and E. Katifori, Global optimization, local adaptation, and the role of growth in distribution networks, *Physical review letters* **117**, 138301 (2016).
- [15] D. Hu and D. Cai, Adaptation and optimization of biological transport networks, *Physical review letters* **111**, 138701 (2013).
- [16] S. Cho, C. Li, and I. E. Grossmann, Recent advances and challenges in optimization models for expansion planning of power systems and reliability optimization, *Computers & Chemical Engineering* **165**, 107924 (2022).
- [17] M. Barthélemy and A. Flammini, Optimal traffic networks, *Journal of Statistical Mechanics: Theory and Experiment* **2006**, L07002 (2006).
- [18] F. Schwabl, *Statistical mechanics* (Springer Science & Business Media, 2006).
- [19] S. Patwardhan, M. Barthelemy, Ş. Erkol, S. Fortunato, and F. Radicchi, Symmetry breaking in optimal transport networks, *Nature Communications* **15**, 3758 (2024).
- [20] M. Durand, Structure of optimal transport networks subject to a global constraint, *Physical Review Letters* **98**, 088701 (2007).
- [21] S. Bohn and M. O. Magnasco, Structure, scaling, and phase transition in the optimal transport network, *Physical review letters* **98**, 088702 (2007).
- [22] F. Kaiser, H. Ronellenfitsch, and D. Witthaut, Discontinuous transition to loop formation in optimal supply networks, *Nature communications* **11**, 5796 (2020).
- [23] F. Kaiser, P. C. Böttcher, H. Ronellenfitsch, V. Latora, and D. Witthaut, Dual communities in spatial networks, *Nature Communications* **13**, 7479 (2022).
- [24] F. Folz, K. Mehlhorn, and G. Morigi, Noise-induced network topologies, *Physical Review Letters* **130**, 267401 (2023).
- [25] M. Newman, *Networks* (Oxford university press, 2018).
- [26] S. Pfenninger and I. Staffell, Long-term patterns of european pv output using 30 years of validated hourly reanalysis and satellite data, *Energy* **114**, 1251 (2016).
- [27] I. Staffell and S. Pfenninger, Using bias-corrected reanalysis to simulate current and future wind power output, *Energy* **114**, 1224 (2016).
- [28] D. Heide, L. Von Bremen, M. Greiner, C. Hoffmann, M. Speckmann, and S. Bofinger, Seasonal optimal mix of wind and solar power in a future, highly renewable europe, *Renewable Energy* **35**, 2483 (2010).
- [29] A. Pepiciello, C. Bernardo, and J. L. Domínguez-García, Modeling of multi-energy systems as multilayer networks, in *2023 IEEE Belgrade PowerTech* (IEEE, 2023) pp. 01–06.
- [30] A. Benigni, A. Monti, S. Schwarz, and M. Milton, A polynomial chaos based tool for multi-energy systems: A sensitivity analysis test case, in *2024 Open Source Modelling and Simulation of Energy Systems (OSMES)* (IEEE, 2024) pp. 1–6.